1521-009X/46/6/897–907$35.00
Drug Metabolism and Disposition

https://doi.org/10.1124/dmd.117.079830
Drug Metab Dispos 46:897–907, June 2018

Predicting Antitumor Effect of Deoxypodophyllotoxin in NCI-H460 Tumor-Bearing Mice on the Basis of In Vitro Pharmacodynamics and a Physiologically Based Pharmacokinetic-Pharmacodynamic Model[S]

Yang Chen,[1] Kaijing Zhao,[1] Fei Liu, Ying Li, Zeyu Zhong, Shijin Hong, Xiaodong Liu,[2] and Li Liu[2]

Center of Drug Metabolism and Pharmacokinetics, School of Pharmacy, China Pharmaceutical University, Nanjing, China

Received December 6, 2017; accepted April 2, 2018

ABSTRACT

Antitumor evaluation in tumor-bearing mouse is time- and energy-consuming. We aimed to investigate whether in vivo antitumor efficacy could be predicted on the basis of in vitro pharmacodynamics using deoxypodophyllotoxin (DPT), an antitumor candidate in development, as a model compound. Proliferation kinetics of monolayer-cultivated NCI-H460 cells under various DPT concentrations were quantitatively investigated and expressed as calibration curves. Koch two-phase natural growth model combined with sigmoid E_{max} model, i.e., $dM/dt = 2\lambda_0\lambda_1 M/(\lambda_1 + 2\lambda_0 M) - E_{max}C^{\gamma}/(EC_{50}^{\gamma} + C^{\gamma})\cdot M$, was introduced to describe cell proliferation (M) against time under DPT treatment (C). Estimated in vitro pharmacodynamic parameters were: EC_{50}, 8.97 nM; E_{max}, 0.820 day^{-1}, and γ, 7.13. A physiologically based pharmacokinetic model including tumor compartment was introduced to predict DPT disposition in plasma, tumor tissue, and main normal tissues of NCI-H460 tumor-bearing mice following a single dose. The in vivo pharmacodynamic model and parameters were assumed the same as the in vitro ones, and linked with simulated tumor pharmacokinetic profiles by a physiologically based pharmacokinetic (PBPK) model to build a PBPK-pharmacodynamic (PBPK-PD) model. After natural growth parameters (λ_0 and λ_1) were estimated, the objective in this study was to predict with the PBPK-PD model the tumor growth in NCI-H460 tumor-bearing mice during multidose DPT treatment, a use of the model similar to what others have reported. In our work, the model was successfully applied to predict tumor growth in SGC-7901 tumor-bearing mice. The resulting data indicated that in vivo antitumor efficacy might be predicted on the basis of in vitro cytotoxic assays via a PBPK-PD model approach. We demonstrated that the approach is reasonable and applicable and may facilitate and accelerate anticancer candidate screening and dose regimen design in the drug discovery process.

Introduction

Deoxypodophyllotoxin (DPT) is one of the main active ingredients in herbs like *Podophyllum emodi, Anthriscus sylvestris,* and *Pulsatilla koreana* (Wong et al., 2000; Khaled et al., 2013). The lignan compound exhibits various pharmacological activities such as antitumor, antiviral, antiplatelet aggregation, and anti-inflammatory effects (Khaled et al., 2013), among which the antitumor effect has received the most attention and is therefore widely characterized (Kim et al., 2002; Shin et al., 2010; Jiang et al., 2013; Hu et al., 2016; Khaled et al., 2016). In China, a phase I clinical trial for DPT has been approved for patients of lung cancer, gastric cancer, and breast cancer—especially those resistant to paclitaxel and etoposide—in an intravenous formulation of β-cyclodextrin inclusion complex.

Several studies have demonstrated that DPT strongly exerts its cytotoxic effect by inhibiting polymerization and promoting depolymerization of tubulin, as well as inducing cell cycle arrest at G2/M phase accompanied by cell apoptosis (Yong et al., 2009; Khaled et al., 2013; Guerram et al., 2015). In vitro experiments have demonstrated that IC_{50} values of DPT against several human cancer cell lines were in the low nanomolar range (13–27 nM), far superior to its analog etoposide (Guerram et al., 2015). Several studies also revealed that the inhibition of specific cell lines by DPT was exposure time- and concentration-dependent (Yong et al., 2009; Jiang et al., 2013; Wang et al., 2015). Furthermore, in vivo antitumor effects of DPT have been illustrated (Wu et al., 2013; Wang et al., 2015; Khaled et al., 2016).

Our previous studies have shown the metabolic kinetics of DPT in hepatic microsomes and its high plasma protein binding in various species (Chen et al., 2016; Xie et al., 2016). Demethylenated metabolite (M2) was shown to be the main metabolite of DPT (Chen et al., 2016; Xie et al., 2016). Subsequently, a whole-body physiologically based

The project was supported by the National Natural Science Foundation of China [No. 81673505, 81573490]; the Natural Science Foundation of Jiangsu Province of China [BK20161457]; and the Priority Academic Program Development of Jiangsu Higher Education Institutions and the Policy Directive Program of Jiangsu Province [BY2015072-03].

[1]Y.C. and K.Z. are co-first authors.

[2]X.L. and L.L. are co-corresponding authors.

https://doi.org/10.1124/dmd.117.079830.

[S]This article has supplemental material available at dmd.aspetjournals.org.

ABBREVIATIONS: AUC_{0-tn}, area under the concentration-time curve from time zero to last time; $AUC_{0-\infty}$, area under the concentration-time curve from time zero to infinity; CL, clearance; CV, coefficient of variation; DPT, deoxypodophyllotoxin; E_{max}, the maximum effect; K_m, Michaelis-Menten constant; $K_{p,T}$, tissue-to-plasma concentration ratio; PBPK, physiologically based pharmacokinetic; PBPK-PD, PBPK-pharmacodynamic; V_{max}, the maximum metabolic velocity; γ, Hill coefficient.

pharmacokinetic (PBPK) model of DPT including main organs of body was established on the basis of in vitro assays (Chen et al., 2016). The developed PBPK model successfully predicted plasma pharmacokinetics of DPT in mice, rats, monkeys, and dogs. Good predictions were also found for pharmacokinetics in tissues of mice (Chen et al., 2016). It is possible to gain a profound understanding of the dynamics of drug disposition in both plasma and tissues/organs through the PBPK model. Thus, making connections between drug exposure in target tissues and its efficacy is facilitated.

The mouse xenograft model of human tumor is an important pharmacological model and essential for antitumor evaluation prior to clinical trials (Kelland, 2004; Ruggeri et al., 2014). Tumor growth inhibition is the most direct and decisive standard for efficacy evaluation, and is easy to quantify continuously. Nevertheless, experiments related to tumor-bearing mouse are time-, energy-, and money-consuming. In vitro evaluation on monolayer-cultured cell proliferation is much more convenient, economical, and reproducible compared with in vivo study. Therefore, it would be worthwhile to predict the antitumor effect in tumor-bearing mouse on the basis of in vitro assays. Even though in vitro data may not interpret in vivo efficacy directly, intrinsic links may exist between in vitro and in vivo pharmacodynamic characteristics. The aim of the present study was to forecast in vivo efficacy on the basis of an in vitro approach through PBPK-pharmacodynamic (PBPK-PD) model establishment, with DPT as a model compound. In vitro proliferation kinetics of NCI-H460 cells (a human non–small-cell lung cancer), a sensitive cell line (Wu et al., 2013), was investigated under different DPT concentrations. In vitro pharmacodynamic models were then established and corresponding parameters estimated. Concentration-time profiles of DPT in plasma, tumor tissue, and normal tissues of NCI-H460 tumor-bearing mice were simultaneously predicted using a developed PBPK model with tumor tissue compartment and further validated by in vivo data. Finally, a PBPK-PD model was developed on the basis of in vitro pharmacodynamic model and parameters, as well as simulated pharmacokinetic profiles in tumor tissue, to predict antitumor effects of DPT in NCI-H460 tumor-bearing mice. The predictions were validated by tumor volume growth data during DPT treatment. In addition, this approach was further confirmed by its application in the SGC-7901 (a human gastric cancer) tumor model. Our work indicates that perturbed tumor growth could be predicted by extrapolating in vitro pharmacodynamics to in vivo circumstance using a PBPK-PD model.

Materials and Methods

Materials. The analytical standards of DPT (purity 99.88%, for in vitro and analytical studies) and its metabolite M2 (purity 99.45%), and β-cyclodextrin inclusion complex of DPT (content 3.36%, for in vivo administrations) were kindly provided by Medicinal and Chemical Institute of China Pharmaceutical University (Nanjing, China). Diazepam (purity 99.9%) used as internal standard was purchased from National Institutes for Food and Drug Control (Beijing, China). Enhanced cell counting kit-8 (cat. no. C0042) and BCA Protein Assay Kit (cat. no. P0012) were purchased from Beyotime Institute of Biotechnology (Nantong, China). Cell culture media, fetal bovine serum, 0.25% trypsin, and rapid equilibrium dialysis device system (12K molecular weight cut-off, cat. no. 90112) were purchased from Thermo Fisher Scientific (Waltham, MA). All the other reagents were commercially available.

NCI-H460 Cell Culture and In Vitro Pharmacodynamic Assay of DPT. NCI-H460 cell line was provided by Type Culture Collection of Chinese Academy of Sciences (Shanghai, China) and authenticated by short-tandem-repeat analysis. Cells were cultured in RPMI-1640 medium (cat. no. 31800022; Gibco/Thermo Fisher Scientific) supplemented with 1.5 g/l $NaHCO_3$, 2.5 g/l glucose, 0.11 g/l sodium pyruvate, antibiotics (62.5 mg/l ampicillin and 100 mg/l streptomycin), and 10% fetal bovine serum (cat. no. 10100147; Gibco), maintained in humidified atmosphere containing 5% CO_2 at 37°C.

Calibration curves for cell counts were established as follows. The cultured cells were digested and resuspended by cell medium. Then the cell suspension was counted by TC10 automated cell counter (Bio-Rad, Hercules, CA) and further diluted for a series of working suspensions with known cell count density (1×10^4–1×10^6 cells/ml) by the medium. An aliquot of each working suspension (100 μl) was seeded in a 96-well plate, and cells were allowed to attach (for about 4 hours). Medium was then gently aspirated and 100 μl no phenol red RPMI-1640 medium (cat. no. 11835030; Gibco) and 10 μl of enhanced cell counting kit-8 reagent were added to each well. The plate was subsequently placed in a cell incubator for 1 hour. The absorbance of each well was obtained at wavelength of 450 nm by microplate reader (BioTek, Winooski, VT) and the calibration curve was established by the regression of absorbances to cell counts in the wells.

For a pharmacodynamic assay, NCI-H460 cells were seeded in 96-well plates at a density of 1000 cells/well and allowed to attach for 24 hours. Cells were then treated with 100 μl of either vehicle (RPMI-1640 medium) or medium containing different concentrations of DPT (5.53, 7.29, 9.80, 13.06, and 17.59 nM) for designated times (0, 12, 24, 36, 48, 60, 72, and 84 hours). Cell counts after treatments were measured by accompanied calibration curves, and the proliferation profiles against time under different DPT exposures were obtained.

In Vitro Pharmacodynamic Model Development. DPT exerts its cytotoxic effect on NCI-H460 cells by triggering necroptosis according to a previous report (Wu et al., 2013). We assumed that cells in different phases of the cell cycle were affected by the compound to the same extent. Therefore, a cell cycle nonspecific cytotoxicity model was used to depict the in vitro cell proliferation kinetics following exposure to DPT (Lobo and Balthasar, 2002):

$$\frac{d\mathrm{M}}{dt} = (k_{ng} - \mathrm{K}) \times \mathrm{M} \tag{1}$$

where M stands for cell count. The proliferation rate is composed of the natural growth and drug effect according to the model. k_{ng} and K stand for the first-order kinetic parameters (unit: day^{-1}) of the two parts above, respectively.

Nevertheless, the exponential equation above might not be suitable for extension to predicting in vivo tumor growth, which usually demonstrates a two-phase growth feature: an initial exponential growth and a following linear growth (Koch et al., 2009). Therefore, to match in vivo circumstance and achieve in vitro-in vivo extrapolation, the natural proliferation of cultured cells without drug perturbation was also described by the two-phase growth model suggested by Koch et al. (2009):

$$\frac{\mathrm{dM}}{\mathrm{dt}} = \frac{2\lambda_0\lambda_1\mathrm{M}}{\lambda_1 + 2\lambda_0\mathrm{M}} \tag{2}$$

where M represents cell count. λ_0 (unit: day^{-1}) and λ_1 (unit: count/d) represent exponential and linear proliferation rate parameters, respectively, and could be obtained by fitting the model to natural cell proliferation data.

When cell proliferation was affected by drug treatment, an inhibitive rate was added to eq. 2 (Yuan et al., 2015; Eigenmann et al., 2016):

$$\frac{\mathrm{dM}}{\mathrm{dt}} = \frac{2\lambda_0\lambda_1\mathrm{M}}{\lambda_1 + 2\lambda_0\mathrm{M}} - \mathrm{K} \cdot \mathrm{M} \tag{3}$$

where K stands for the first-order inhibitive parameter (unit: day^{-1}).

DPT exhibits a sigmoid maximum effect (E_{max}) pharmacodynamic characteristic against NCI-H460 cell line in the previous study (Wu et al., 2013). Accordingly, K in eqs. 1 and 3 could be expressed as follows:

$$\mathrm{K} = \frac{E_{\max} \times C^{\gamma}}{EC_{50}^{\gamma} + C^{\gamma}} \tag{4}$$

where C represents DPT concentration (unit: nM), and E_{max} (unit: day^{-1}), EC_{50} (unit: nM), and γ are the in vitro pharmacodynamic parameters of DPT.

The two models (eqs. 1 and 3) were fitted to the cell proliferation profiles obtained above, respectively, and corresponding in vitro parameters were estimated.

Tumor Xenograft Model. BALB/$c^{nu/nu}$ nude mice (half males and half females) were purchased from Cavens Laboratory Animal Co., Ltd. (Changzhou, China). The animals were housed in a specific-pathogen–free environment under

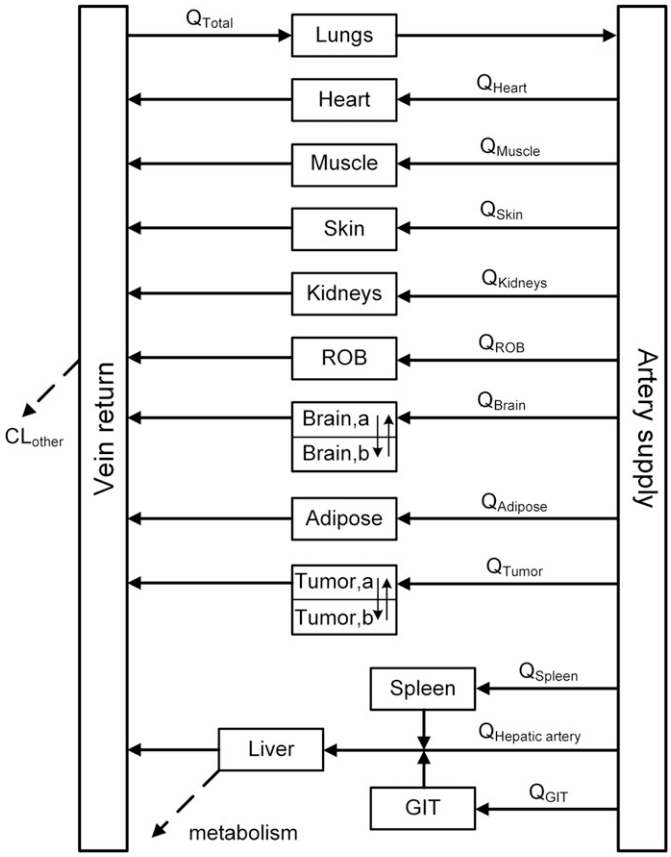

Fig. 1. Schematic diagram of PBPK model of DPT in tumor-bearing mouse. a and b represent vascular and extravascular compartment, respectively. CL_{other} represents clearance of extrahepatic elimination. Q and solid arrows represent blood flow. GIT, gastrointestinal tract; ROB, rest of body.

constant temperature (25–28°C) and humidity (50%–60%), with 12-hour light/dark cycle. Rodent chow and water were autoclaved and provided ad libitum. Animal experiments were carried out according to the *Guide for the Care and Use of Laboratory Animals* and approved by Animal Ethics Committee of China Pharmaceutical University, No. CPU-PCPK-14311010078.

The nude mice of about 4–6 weeks of age (weight: 18–22 g) were inoculated with tumor cell suspension subcutaneously (2×10^6 cells/mouse) in the right flank region. Tumor diameters from two perpendiculars (a, length; b, width) were measured by a vernier caliper and tumor volume (V, unit: cm^3) was calculated according to the equation: $V = (a \times b^2)/2$. (Magni et al., 2006; Salphati et al., 2010).

Pharmacokinetic Study in NCI-H460 Tumor-Bearing Mice. When the mean tumor volume reached 500 mm^3, 108 mice were randomly divided into two groups and received a single dose of DPT of 6.25 or 25 mg/kg via tail veins, respectively. The mice were fasted overnight prior to dosing. DPT in β-cyclodextrin inclusion complex was dissolved in 0.9% normal saline within 2 hours before administration. Six mice (three males and three females) from each group were sacrificed at 2, 5, 10, 20, 45, 60, 120, 240, and 480 minutes postdose, respectively. For each mouse, a blood sample was collected into a heparinized tube and centrifuged for 5 minutes at 8000*g* to obtain plasma. Tumor tissues were simultaneously removed and weighed. Distributions of DPT in heart, liver, lung, kidney, brain, muscle, and intestine of tumor-bearing mice at 5, 20, 60, and 120 minutes following intravenous dose (25 mg/kg) were also investigated. The tissues including tumors were homogenized in pure water (1:5, w/v). The plasma and tissue homogenate samples were stored at −70°C until analysis, in which DPT concentrations were measured by a liquid chromatography–tandem mass spectrometry method previously described (Liu et al., 2016).

Another eight tumor-bearing mice without DPT administration were sacrificed for blank plasma and liver. Hepatic microsomes were prepared according to a procedure previously described (Chen et al., 2011). Blank plasma from the eight mice was pooled for the protein binding study. The hepatic microsomes and plasma were kept at −70°C until use.

M2 is the main metabolite of DPT in hepatic microsomes of mouse, rat, monkey, dog, and human (Chen et al., 2016; Xie et al., 2016). Preliminary experiment also showed that for 200 nM of DPT following 15-minute incubation in liver microsomes of NCI-H460 tumor-bearing mice (0.05 mg protein/ml), 80.3% of the disappeared DPT was metabolized to M2. Therefore kinetic parameters of M2 formation from DPT in hepatic microsomes were investigated to characterize DPT metabolism in tumor-bearing mice. The composition of the microsomal incubation mixture and the incubation procedure were the same as in the previous report (Xie et al., 2016). A series of DPT concentrations (0.0471–3.02 μM) were used. Microsomal protein level and incubation time were set to 0.01 mg/ml and 5 minutes, respectively. M2 formation in the incubation system was measured on the basis of a previously described method (Xie et al., 2016). Metabolic kinetic parameters of M2 formation were estimated for each animal individual.

Plasma protein binding of DPT in tumor-bearing mouse was evaluated by a method previously described using a rapid equilibrium dialysis device (Chen et al., 2016). Initial DPT concentration in plasma was set to 1.0 μg/ml. Evaluations were carried out in triplicate.

PBPK Model Development. A whole-body PBPK model of DPT for tumor-bearing mouse was constructed as the same scheme in the previous report (Chen et al., 2016) except that a tumor compartment was included (Fig. 1). The body weight of tumor-bearing mouse was assumed to be 20 g. Volume and blood flow rate of each normal organ compartment of tumor-bearing mouse were considered the same as normal mouse (Chen et al., 2016) (Table 1). It was assumed that DPT was mainly eliminated in the liver by transformation to M2, and disposition of DPT in most tissues was illustrated by a perfusion-rate–limited model. The detailed differential equations for normal tissues are described in Supplemental Methods.

An assumption that unbound tissue-to-plasma concentration ratio of DPT was identical across species has given good predictions for pharmacokinetics in various species (Chen et al., 2016). Thus, tissue-to-plasma concentration ratio ($K_{p,T}$) values of DPT in normal tissues of tumor-bearing mouse were derived from those of rats ($K_{p,T,\ rat}$) by the equation: $K_{p,T} = K_{p,T,\ rat} \times f_u/f_{u,\ rat}$, where f_u and $f_{u,\ rat}$ are unbound fractions of DPT in plasma of tumor-bearing mouse and rat, respectively. $K_{p,T,\ rat}$ and $f_{u,\ rat}$ were cited from our previous study (Chen et al., 2016). Calculated $K_{p,T}$ values of tumor-bearing mouse are summarized in Table 1.

Pharmacokinetic profiles of DPT in plasma, tumor, and main normal tissues were predicted by the developed PBPK model, and corresponding pharmacokinetic parameters of predicted profiles were also estimated by noncompartmental analysis. The predictions were then compared to observed data to validate the

TABLE 1

Physiologic parameters for tumor-bearing mouse (20 g) used in PBPK model

	Volume[a]	Blood Flow Rate[a]	$K_{p,T}$[b]
	ml	*ml/min*	
Adipose	1.73	0.72	19.59
Liver	1.10	1.94	1.52
Muscle	7.67	0.91	0.68
Lungs	0.15	8.14 (Cardiac output)	1.55
Kidneys	0.33	1.30	1.28
Brain	0.33	0.26	2.51
Heart	0.10	0.28	0.88
Spleen	0.07	0.09	0.96
Skin	3.30	0.41	1.29
Gastrointestinal tract	0.85	1.50	0.91
Tumor[c]	0.50	0.14	4.23
Rest of body	3.39	2.18	0.0090
Vein	0.65	\	\
Artery	0.33	\	\

[a]Volume and blood flow rates of normal tissues were cited from the previous report (Chen et al., 2016).

[b]$K_{p,T}$ of normal tissues were calculated from the values of rat ($K_{p,T,\ rat}$) (Chen et al., 2016) on the basis of the equation $K_{p,T} = K_{p,T,\ rat} \cdot f_u/f_{u,\ rat}$, where f_u and $f_{u,\ rat}$ mean unbound fraction of DPT in plasma of tumor-bearing mouse and rat, respectively.

[c]Tumor volume came from the actual volume. Blood flow rate of tumor was cited from the previous report (Zhang et al., 2013). $K_{p,T}$ value of tumor was calculated from the $AUC_{0-\infty}$ ratio between tumor tissue and plasma of 6.25 mg/kg single intravenous dose group.

model. Accuracy of prediction was evaluated by fold-error (Chen et al., 2016). Predicted value within a 2-fold error of observed value was considered acceptable (Parrott et al., 2005; Guest et al., 2011).

In Vivo Pharmacodynamics Prediction by PBPK-PD Model. DPT concentration profiles in tumor tissue of tumor-bearing mice during multiple-dose treatment were simulated using the validated PBPK model. The profiles were further connected to in vitro pharmacodynamics of DPT and the characteristics of tumor natural growth to predict the antitumor effect in NCI-H460 tumor-bearing mice. In vitro evaluation of the NCI-H460 cell line also showed that the main metabolite, M2, had no antitumor effect ($IC_{50} > 100$ μM, 72 hours), indicating that the antitumor effect was mainly attributable to DPT.

Tumor growth with drug intervention is illustrated by both eqs. 5 and 6, which are similar to eqs. 1 and 3 describing in vitro pharmacodynamics of DPT, respectively:

$$\frac{dV}{dt} = \mathrm{k_{ng}} \times V - \frac{E_{\max} \times C_f^{\gamma}}{EC_{50}^{\gamma} + C_{\mathrm{f}}^{\gamma}} \times V \quad (5)$$

$$\frac{dV}{dt} = \frac{2\lambda_0\lambda_1 \mathrm{V}}{\lambda_1 + 2\lambda_0 V} - \frac{E_{\max} \times C_f^{\gamma}}{EC_{50}^{\gamma} + C_{\mathrm{f}}^{\gamma}} \times V \quad (6)$$

where V represents tumor volume (unit: ml); k_{ng} (unit: day^{-1}) represents exponential natural growth parameter; and λ_0 (unit: day^{-1}) and λ_1 (unit: ml/d) represent exponential and linear growth rate parameters of natural growth, respectively. The two equations were fitted to tumor volume growth data without DPT treatment, respectively, to yield in vivo k_{ng}, λ_0, and λ_1. Values of in vivo pharmacodynamic parameters E_{max} (unit: day^{-1}), EC_{50} (unit: nM), and γ of DPT were assumed to equal corresponding in vitro estimated values. C_f is free DPT concentration (unit: nM) in tumor tissue and could be simulated dynamically by PBPK model. Consequently, tumor volume growth curves against time during DPT treatment could be obtained by solving the differential equations in the PBPK-PD model.

All mathematical models above were coded and solved by Phoenix WinNonlin software (version 7.0; Certara, Co., Princeton, NJ). Parameter estimations were also conducted on the software.

Validation of Pharmacodynamics Prediction in NCI-H460 Tumor-Bearing Mice. As tumor volumes reached about 100 mm^3, 18 tumor-bearing mice were randomized into three groups (three males and three females in each group), namely, vehicle control, 6.25-mg/kg DPT, and 25-mg/kg DPT treatment groups. DPT or vehicle was administered via tail veins every 3 days for eight doses in total. Body weights and tumor volumes were measured every other day. The day of first administration was designated as time zero. Predicted tumor growth curves during DPT treatment by the developed PBPK-PD model were compared with the observations. Predictive fold-error within 2 denoted success.

Another dataset from a previous report (Wu et al., 2013) was used to further validate the developed PBPK-PD model. Doses of DPT were set to 5, 10, and 20 mg/kg, respectively, which were administered to NCI-H460 tumor-bearing mice three times a week. Values for λ_0 and λ_1 were also estimated using the tumor growth curve of the vehicle control group. Tumor growth curves during DPT treatment were predicted by the developed PBPK-PD model and validated by reported observations (Wu et al., 2013).

PBPK-PD Model Application in SGC-7901 Tumor-Bearing Mice. The developed PBPK-PD model was further applied to predict the antitumor effect of DPT in SGC-7901 tumor-bearing mice. The SGC-7901 cell line was provided by Type Culture Collection of Chinese Academy of Sciences (Shanghai, China) and cultured as described above. For in vitro pharmacodynamic studies, SGC-7901 cells were seeded in 96-well plates at a density of 3000 cells/well and allowed to attach for 24 hours. Cells were then treated with 100 μl of either vehicle (RPMI-1640 medium) or the medium containing different concentrations of DPT (2.57, 3.22, 4.02, 5.02, and 6.28 nM) for designated times (0, 12, 24, 36, 48, 60, 72, and 84 hours). Cell counts were measured using calibration curves of SGC-7901 cells. Corresponding in vitro pharmacodynamic parameters of DPT were estimated using the Koch two-phase model combined with the sigmoid E_{max} model (eq. 3).

It was assumed that the PBPK model structure and parameters of DPT were the same in SGC-7901 and NCI-H460 tumor-bearing mouse. The concentration profiles of DPT in tumor and plasma of SGC-7901 tumor-bearing mouse were predicted and compared with observed data following a single intravenous dose of DPT (6.25 mg/kg). Eighteen male SGC-7901 tumor-bearing mice were randomly divided into six time groups and were sacrificed at 6, 20, 30, 60, 120, 480 minutes postdose, respectively. Plasma and tumor samples were obtained, in which DPT concentrations were measured as described above.

In vivo antitumor effect data of DPT in SGC-7901 tumor-bearing mice were cited from a previous report (Wang et al., 2015). The mice were intravenously given vehicle, 5, 10, and 20 mg/kg of DPT (three times a week), respectively, and tumor volumes were measured for 17 days. λ_0 and λ_1 values for SGC-7901 tumor growth were estimated using tumor growth curve of vehicle group. On the basis of the combination of predicted tumor concentration profiles and estimated in vitro pharmacodynamic parameters, tumor growth profiles in SGC-7901 tumor-bearing mice during DPT treatment were predicted by the PBPK-PD model and compared with reported observations (Wang et al., 2015).

Results

In Vitro Pharmacodynamics of DPT against NCI-H460 Cell Line. To quantify cell counts, calibration curves were established on five consecutive days with desirable precision as $y = (0.0951 \pm 0.0083)\,x - (0.0030 \pm 0.0038)$ ($r^2 > 0.9918$), where y and x stand for absorbance and cell count ($\times 10^4$), respectively (Fig. 2). The proliferation of NCI-H460 cells against time under different concentrations of DPT is depicted in Fig. 3. The results show that DPT concentration-dependently exerted its potent cytotoxic effect on the tumor cell line. A sharp concentration-effect relationship was observed, which obeyed sigmoid E_{max} model. DPT scarcely exhibited its cytotoxic effect at 5.53 nM, but at 13.06 nM the maximum effect was nearly reached and proliferation was almost inhibited thoroughly. Both cell cycle nonspecific cytotoxicity model (model A, eq. 1) and the cytotoxicity model extended from two-phase Koch model (model B, eq. 3) were fitted to the cell proliferation curves (Fig. 3). Estimated in vitro pharmacodynamic parameters of the two models were listed in Table 2.

It could be seen from Fig. 3 and Table 2 that both models seemed to well characterize the cell proliferation, and similar estimated results were obtained. The estimated EC_{50} values coincided with the values previously reported (Wu et al., 2013). Therefore, both models along with their pharmacodynamic parameters were used to attempt a forecast of in vivo tumor growth.

Pharmacokinetics of DPT in NCI-H460 Tumor-Bearing Mice. DPT showed high affinity to plasma protein of tumor-bearing mouse. The evaluated protein binding value using a rapid equilibrium dialysis approach was 95.12% ± 0.42%, which was slightly lower than that in normal mouse (97.17% ± 0.25%) (Chen et al., 2016).

The kinetic profiles of M2 formation from DPT in hepatic microsomes of tumor-bearing mice were studied, and they obeyed typical Michaelis-Menten kinetics judged by corresponding Eadie-Hofstee plots. The estimated maximum metabolic velocity (V_{max}), Michaelis-Menten constant (K_m), and calculated intrinsic clearance ($CL_{int} = V_{max}/K_m$) were 1.22 ± 0.55 nmol/min per milligram protein, 0.32 ± 0.06 μM, and 4.07 ± 2.19 ml/min per milligram protein, respectively ($n = 8$). The calculated intrinsic clearance in hepatic microsomes from tumor-bearing mice was higher than that from normal mice (1.89 ml/min per milligram protein) (Xie et al., 2016).

Pharmacokinetic profiles of plasma, tumor, and normal tissues in tumor-bearing mice were obtained following a single intravenous dose of DPT. The results showed that in plasma, DPT was eliminated rapidly following administration, with a half-life of about 50 minutes (Fig. 4A; Table 3). In tumor, DPT concentration reached its peak rapidly, but elimination was slower than in plasma, with half-lives of 157 and 205 minutes in 6.25 mg/kg and 25 mg/kg dose groups, respectively. (Fig. 4B; Table 3). The exposure of DPT in tumor was about four times higher than in plasma (Table 3), demonstrating that high affinity existed between the drug molecule and tumor tissue. In addition, DPT showed very high plasma clearances (2.73 and 2.77 ml/min, Table 3) exceeding liver blood flow rate (1.94 ml/min, Table 1), indicating the existence of extrahepatic elimination.

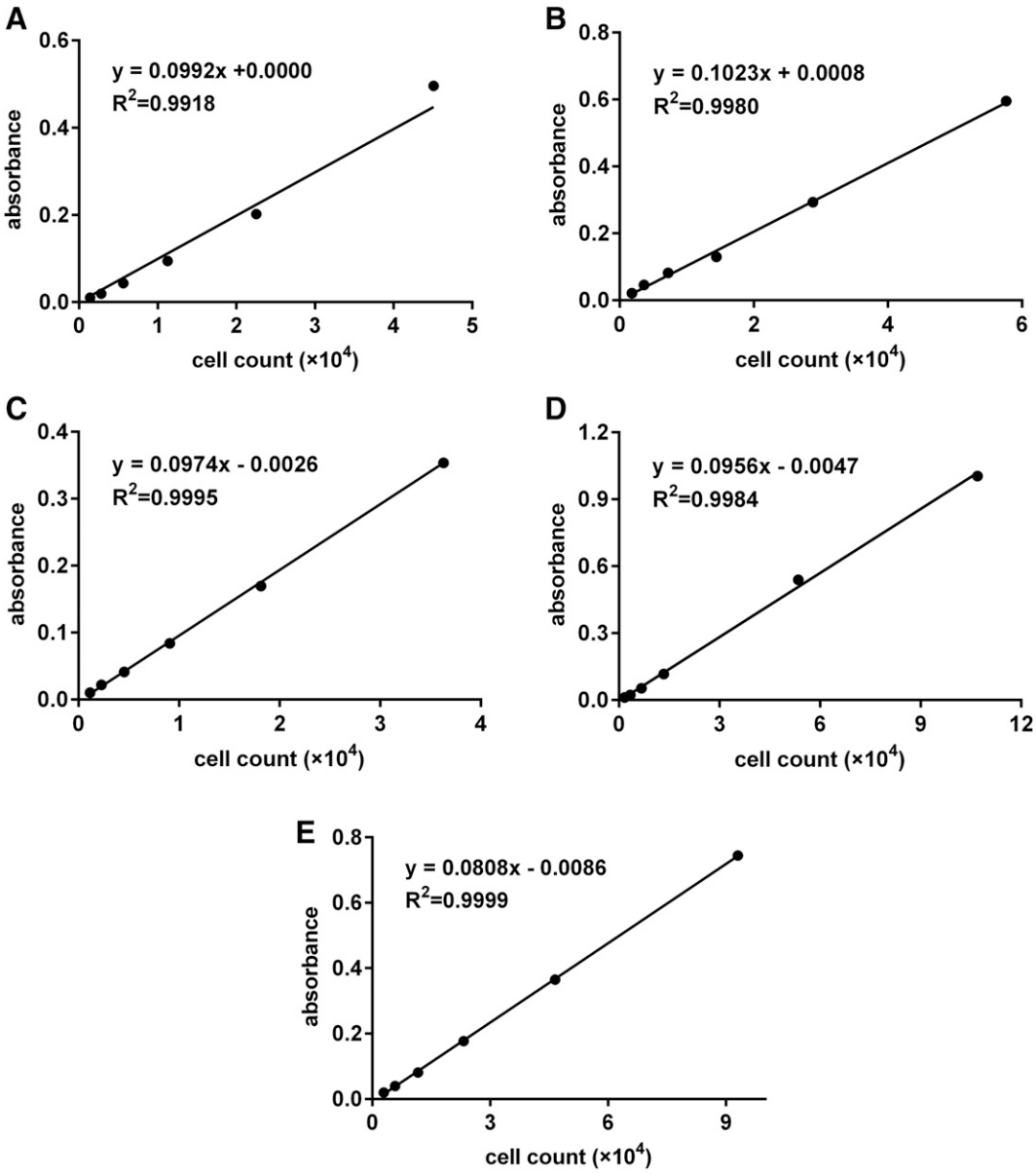

Fig. 2. The calibration curves to determine cultured NCI-H460 cell counts on 5 consecutive days (A–E).

PBPK Model Validation in NCI-H460 Tumor-Bearing Mice. As mentioned above, extrahepatic elimination might occur somewhere, so an additional clearance (CL_{other}) was introduced into the venous compartment of PBPK model (Fig. 1). CL_{other} was calculated with the following equation on the basis of a well-stirred model:

$$CL_{other} = CL_{\text{in vivo}} - \frac{Q \times f_u \times (V_{max}/K_m) \times PBSF}{Q + f_u \times (V_{max}/K_m) \times PBSF} \quad (7)$$

where $CL_{in\ vivo}$ is the in vivo clearance estimated by plasma pharmacokinetic profile following intravenous dose of DPT (6.25 mg/kg), whose value was 2.73 ml/min (Table 3). Q is liver blood flow rate (1.94 ml/min, Table 1). f_u, physiologically based scaling factor *(PBSF)*, V_{max}, and K_m are unbound fraction of DPT in plasma, total hepatic microsomal protein amount [49.28 mg protein/mouse, assuming the same as normal mice (Chen et al., 2016)], and kinetic parameters of M2 formation from DPT in hepatic microsomes of tumor-bearing mice, respectively. Therefore, CL_{other} was calculated to be 1.11 ml/min.

Pharmacokinetic study showed that DPT concentration-time profiles in tumor tissue did not synchronize with those in plasma, exhibiting an obvious increase before elimination. Therefore, permeability-limited model was adopted for illustrating disposition of DPT in tumor tissue as follows:

$$V_a \frac{dC_a}{dt} = Q_{Tumor} \times (C_A - C_a) - PS_{Tumor}(C_a - C_b/K_{p,Tumor}) \quad (8)$$

and

$$V_b \frac{dC_b}{dt} = PS_{Tumor} \times (C_a - C_b/K_{p,Tumor}) \quad (9)$$

where subscript a and b represent vascular and extravascular compartment, which were assumed to account for 10% and 90% of the total

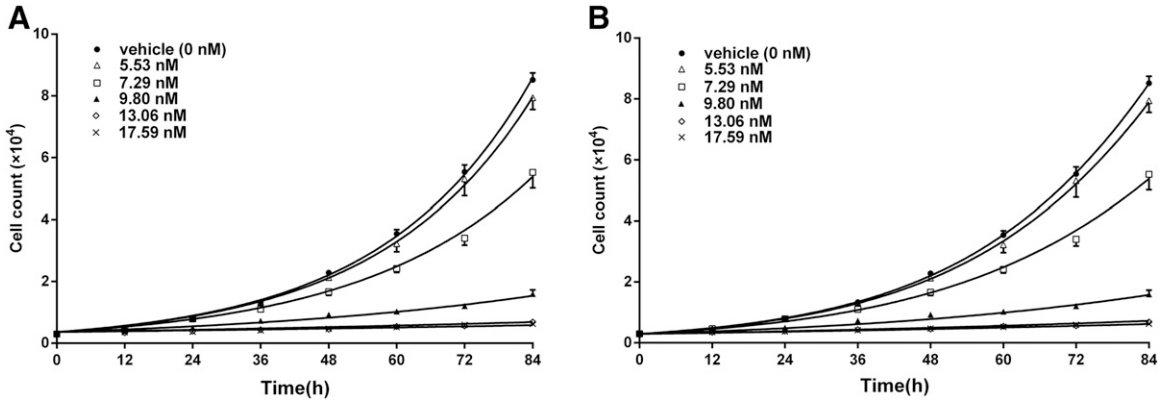

Fig. 3. The observed (symbol) and fitted (line) proliferation profiles of NCI-H460 cells under various concentrations of DPT by cell cycle nonspecific cytotoxicity model (A) and the cytotoxicity model extended from two-phase Koch model (B). Symbols represent mean ± S.D. (n = 5) of cell counts determined by calibration curves.

tumor volume (0.5 ml), respectively (Zhang et al., 2013). C (unit: nM) and V (unit: ml) are DPT concentration and volume of related compartment, respectively. C_A (unit: nM) means the drug concentration in arterial blood compartment. Tumor-to-plasma concentration ratio of DPT ($K_{p,Tumor}$) was 4.23, calculated from the $AUC_{0-\infty}$ ratio between tumor tissue and plasma of the 6.25-mg/kg dose group (Table 3). Permeability-surface product of tumor (PS_{Tumor}) was estimated to be 0.0116 ml/min (CV: 9.48%) by fitting the model to tumor concentration-time profile of the 6.25-mg/kg dose group, which was successfully validated by the profile of the 25-mg/kg dose group. Blood flow rate of tumor (Q_{Tumor}) was assumed to be 0.14 ml/min (Zhang et al., 2013), and cardiac output of tumor-bearing mouse was set to be the sum of blood flow rates of all organs, including tumor (Table 1).

Pharmacokinetic profiles of DPT in plasma and tumor tissue of tumor-bearing mice following a single intravenous dose of DPT (6.25 and 25 mg/kg) were predicted using the developed PBPK model and compared with the observed data. Acceptable results were obtained that most of predicted concentrations and all corresponding pharmacokinetic parameters of the predicted profiles fell within 2-fold error of observed values (Fig. 4C; Table 3).

Concentration-time profiles of DPT in main normal tissues of tumor-bearing mice following a single intravenous dose of DPT (25 mg/kg) were simultaneously predicted by PBPK model and compared with observed data. The area under concentration-time curve from 0 to 120 minute ($AUC_{0-120\ minutes}$) in tissues was also estimated. The results showed that predicted $AUC_{0-120\ minutes}$ of DPT in main normal tissues were within 2-fold error of observations, except in lungs (Fig. 5).

The validations by profiles of plasma, tumor, and normal tissues showed that the developed PBPK model could predict DPT disposition in tumor-bearing mice following a single intravenous dose. This result suggested that DPT concentration profile in tumor tissue during multidose treatment might also be simulated accurately by the model.

TABLE 2

Estimated in vitro pharmacodynamic parameters of DPT against NCI-H460 cell line using cell cycle nonspecific cytotoxicity model (A) and the cytotoxicity model extended from two-phase Koch model (B)

Data in parentheses denote corresponding CV.

	Model A	Model B
k_{ng} (day^{-1})	0.905 (1.56%)	\
λ_0 (day^{-1})	\	0.521 (2.73%)
λ_1 (count/day)	\	3.08×10^5 (17.8%)
EC_{50} (nM)	9.07 (1.04%)	8.97 (0.864%)
E_{max} (day^{-1})	0.775 (2.53%)	0.820 (2.04%)
γ	7.16 (3.10%)	7.13 (2.68%)

Validation of Pharmacodynamics Prediction in NCI-H460 Tumor-Bearing Mice. Perturbed tumor growth curves by DPT in NCI-H460 tumor-bearing mice were predicted by the established PBPK-PD model. During DPT treatment, tumor volume was an increasing variable against time instead of a fixed value. Accordingly, blood flow rate and permeability-surface product of tumor were assumed to be proportional to tumor volume. Body weight of mouse (regardless of tumor weight) and other parameters in the PBPK-PD model were assumed constant as tumor volume increased. C_f (free DPT concentration in tumor tissue, unit: nM) was obtained by the equations $C_f = f_{u,tumor} \times C_{tumor}$ and $f_{u,tumor} = f_u/K_{p,tumor}$ (Maurer et al., 2005), where C_{tumor}, $f_{u,tumor}$, f_u, and $K_{p,tumor}$ are DPT concentration in tumor tissue (extravascular compartment, unit: nM), unbound fraction of DPT in tumor tissue and in plasma, and tumor-to-plasma concentration ratio of DPT, respectively. C_{tumor} was simulated dynamically by the PBPK model above.

In vivo studies demonstrated the significant antitumor effect of DPT in a dose-dependent manner (Fig. 6, A and B). In vivo tumor growth profiles in the present study were predicted using both eqs. 5 and 6, respectively (Supplemental Fig. 1). The results showed that two-phase Koch model (eq. 6) better simulated tumor growth than an exponential model (eq. 5) with lower AIC values (−40.3 vs. −12.9 for 6.25 mg/kg; −51.5 vs. −21.9 for 25.0 mg/kg) and a higher correlation coefficient (R: 0.9912 vs. 0.9437). Therefore, the Koch two-phase natural growth model combined with sigmoid E_{max} model (eq. 6) was selected as the final model to characterize in vitro pharmacodynamics as well as predict in vivo pharmacodynamics of DPT.

In eq. 6, kinetic parameters λ_0 and λ_1 in Fig. 6A were estimated to be 0.110 day^{-1} (CV: 26.8%) and 0.0797 ml/d (CV: 16.3%), respectively, by tumor growth curve of the vehicle control group. Tumor growth curves in Fig. 6A during DPT treatment (6.25 and 25 mg/kg, once every 3 days) were predicted by the developed PBPK-PD model and compared with observations. Predicted curves were in good accordance with the observed data (Fig. 6A). Data previously reported (Fig. 6B, Wu et al., 2013) were also used to validate the developed PBPK-PD model, of which λ_0 and λ_1 were estimated to be 0.426 day^{-1} (CV: 22.5%) and 0.142 ml/d (CV: 8.64%), respectively, by tumor growth curve of vehicle control group in Fig. 6B. Acceptable prediction of tumor growth curves in Fig. 6B during DPT treatment (5, 10, and 20 mg/kg, three times a week) was also obtained. Predictive fold-errors of tumor volumes in both datasets were all less than 2 (Fig. 6, C and D). Successful validations by

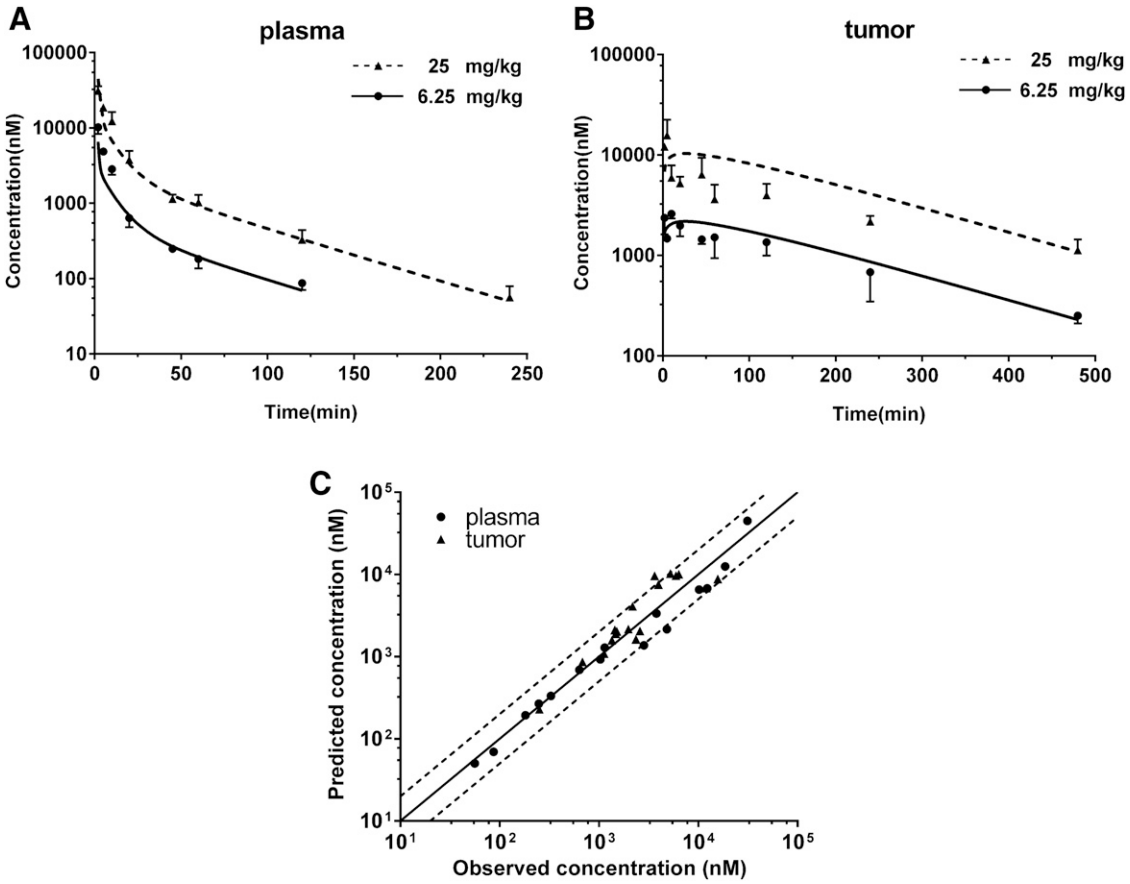

Fig. 4. Observed (symbol) and predicted (line) concentration-time profiles of DPT by the developed PBPK model in plasma (A) and tumor (B) of NCI-H460 tumor-bearing mice following a single intravenous dose. Symbols represent mean ± S.D. (n = 6) of observations. (C) Relationship between mean observed and predicted DPT concentrations in plasma and tumor of the two dose groups above at each time point. Solid and dashed lines indicate unity and 2-fold errors of prediction, respectively.

external data from multifaceted sources indicated the predictive accuracy and rationality of the developed PBPK-PD model.

PBPK-PD Model Application in SGC-7901 Tumor-Bearing Mice. The Koch two-phase natural growth model combined with sigmoid E_{max} model was also used to characterize the in vitro proliferation profiles of SGC-7901 cells under DPT exposure (Fig. 7A). The estimated in vitro pharmacodynamic parameters were: λ_0: 0.341 day^{-1} (CV: 16.4%); λ_1: 46,296 count/d (CV: 52.1%); EC_{50}: 6.23 nM (CV: 13.1%); E_{max}: 1.02 day^{-1} (CV: 33.5%); and γ: 4.74 (CV: 12.5%).

The predicted pharmacokinetic profiles by the established PBPK model well matched the observations both in plasma and tumor tissues of SGC-7901 tumor-bearing mice after a single intravenous dose (6.25 mg/kg), with predictive fold-errors of all concentrations less than 2 (Fig. 7B). It indicated that the developed PBPK model might be expected to simulate pharmacokinetics of DPT in SGC-7901 xenograft models.

In vivo SGC-7901 tumor growth profiles during DPT administration were predicted on the basis of the estimated in vitro pharmacodynamic parameters, simulated tumor concentration profiles, and estimated tumor natural growth parameters (λ_0 = 0.257 day^{-1}, CV = 210%; λ_1 = 0.0589 ml/d, CV = 42.1%). The predicted profiles were consistent with observed data (Wang et al., 2015) (Fig. 7C). All predicted relative tumor volumes fell within a 2-fold error (Fig. 7D). The successful prediction further demonstrated the applicability of the developed PBPK-PD model in xenograft models.

TABLE 3

Comparison of pharmacokinetic parameters of DPT in plasma and tumor of NCI-H460 tumor-bearing mice following a single intravenous dose estimated from observed and predicted concentration-time profiles by the developed PBPK model

		Plasma		Tumor	
		6.25 mg/kg	25 mg/kg	6.25 mg/kg	25 mg/kg
AUC_{0-tn} (μM·min)	Obs	108.47	449.85	428.62	1387.99
	Pred	86.11	440.68	490.05	2322.46
$AUC_{0-\infty}$ (μM·min)	Obs	114.90	453.42	485.60	1720.75
	Pred	90.30	443.84	531.81	2520.70
CL (ml/min per kilogram)	Obs	136.68	138.54	/	/
	Pred	173.91	141.52	/	/
V_{ss} (l/kg)	Obs	3.30	3.53	/	/
	Pred	4.06	3.33	/	/
$t_{1/2}$ (min)	Obs	51.21	43.96	156.96	204.67
	Pred	41.83	43.60	126.38	126.38
C_{max} (μM)	Obs	/	/	2.59	15.67
	Pred	/	/	2.18	10.33

C_{max}, maximum concentration; Obs, observed; Pred, predicted; $t_{1/2}$, terminal half-life; V_{ss}, apparent volume of distribution at steady state.

Discussion

As a promising antitumor candidate, DPT shows potent cytotoxic effects both in vitro and in vivo. However, the intrinsic relationship between its in vitro and in vivo pharmacodynamics has not been explored. The main contribution of the present study was the development of a PBPK-PD model for revealing in vitro-in vivo pharmacodynamic

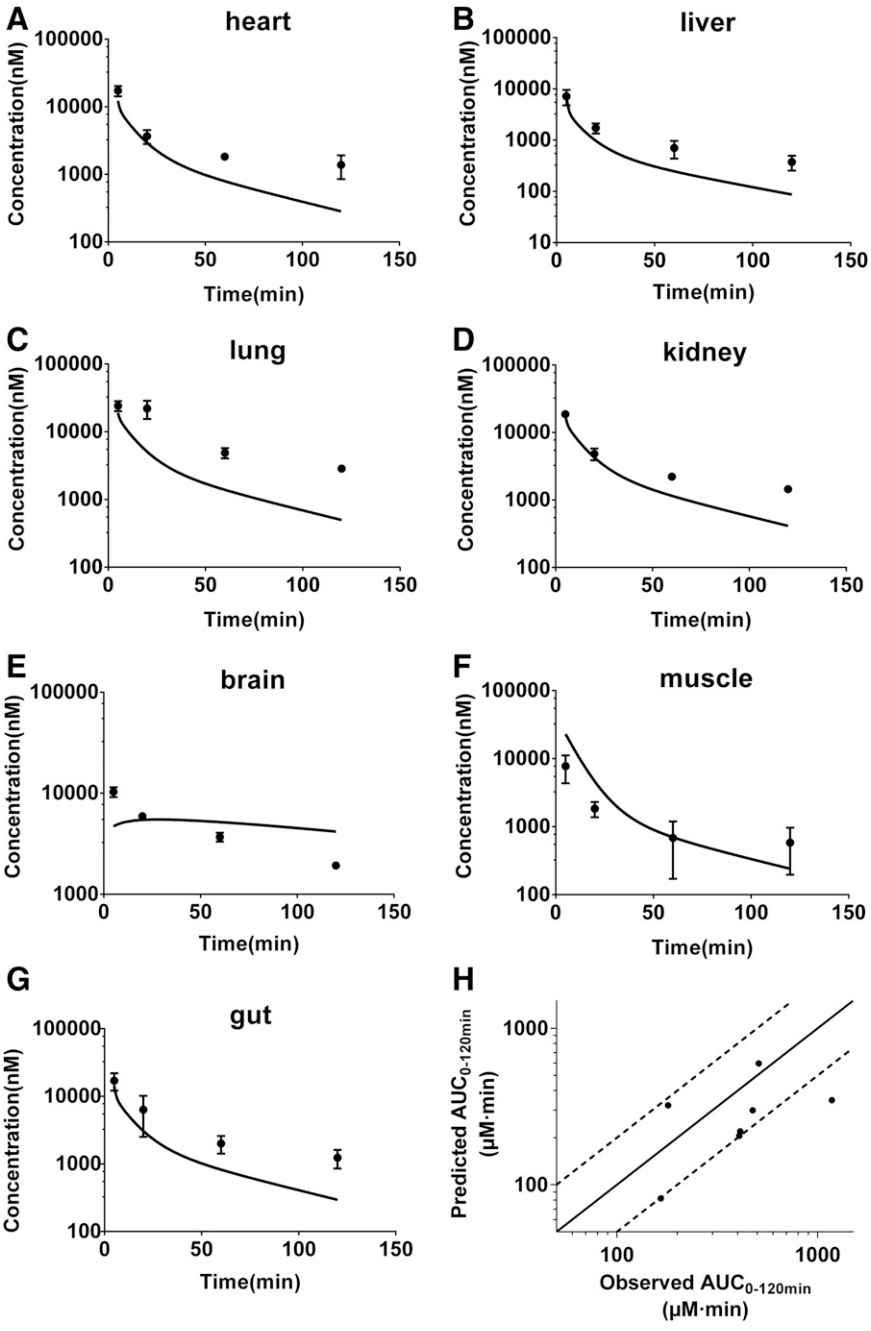

Fig. 5. Observed (symbol) and predicted (line) concentration-time profiles of DPT by the developed PBPK model in heart (A), liver (B), lung (C), kidney (D), brain (E), muscle (F) and gastrointestinal tract (G) of NCI-H460 tumor-bearing mice following a single intravenous dose (25 mg/kg). Symbols represent mean ± S.D. ($n = 6$) of observations. (H) Relationship between observed and predicted $AUC_{0–120\ minutes}$ of DPT in the tissues above. Solid and dashed lines indicate unity and 2-fold errors of prediction, respectively.

correlation and predicting antitumor efficacy in tumor-bearing mice on the basis of in vitro pharmacodynamics. The model approach was validated by a multitumor model, indicating its potential application in antitumor drug discovery.

In general, in vitro antitumor activities of cytotoxic candidates like DPT are evaluated by static methods. Inhibition rates of cell proliferation following designed exposure times under different drug concentrations are obtained and IC_{50} values are estimated (Kim et al., 2002; Jiang et al., 2013; Wu et al., 2013; Guerram et al., 2015). By that approach, estimated IC_{50} values of DPT against NCI-H460 cell line varied from 7.51 to 9.40 nM in our study, depending on exposure time from 24 to 84 hours. This parameter could not reflect the drug effect dynamically, and the variation could have misled our evaluation of the candidate. Therefore, a dynamic function quantitatively describing the cell count–time-concentration relationship of DPT was needed rather than a static one. Several in vitro dynamic models for cytotoxic compounds exist, including a cell cycle specific/nonspecific model and a transit compartment model (Jusko, 1971; Jusko, 1973; Sun and Jusko, 1998; Mager and Jusko, 2001). Since in vivo tumor growth usually does not obey typical exponential features, the in vitro cycle specific/nonspecific model seemed unsuitable for extrapolation to in vivo circumstances. Our study also showed that although an exponential model well described in vitro profiles, it unsatisfactorily characterized in vivo tumor growth. The time delay of the cytotoxic effect of DPT was not observed in our preliminary in vitro assays (data not shown), indicating that the transit compartment model might also have been inappropriate. Consequently, we attempted a two-phase Koch model, along with an inhibitive term related to the cytotoxic candidate, which

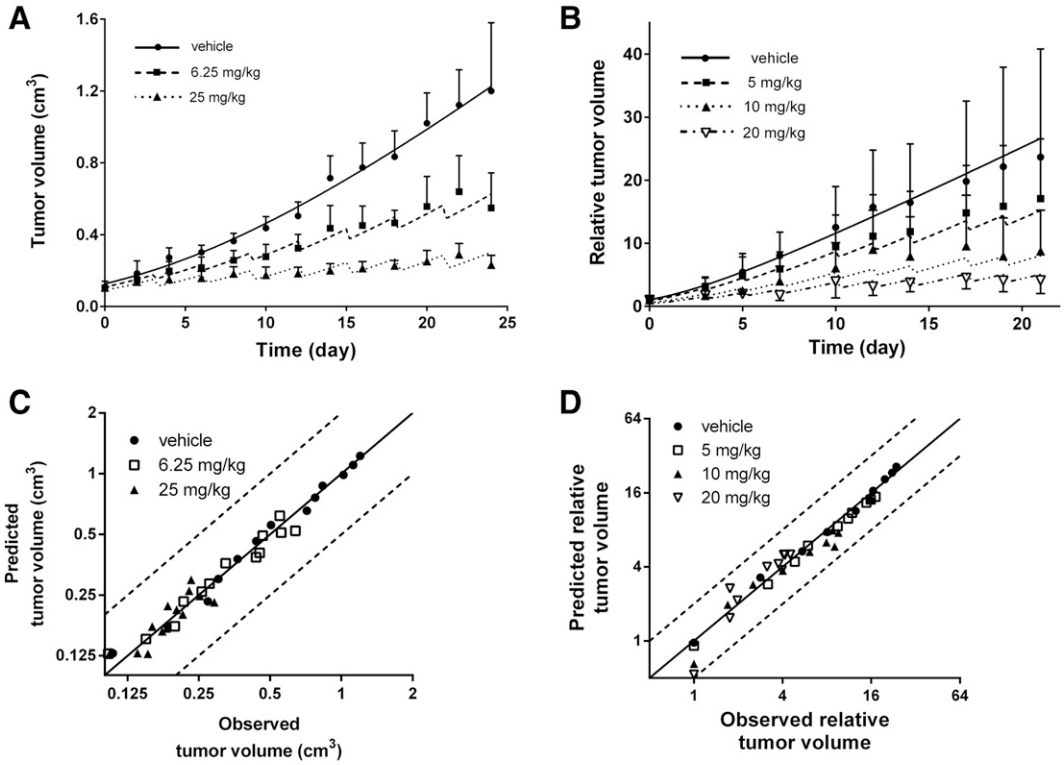

Fig. 6. PBPK-PD model prediction in NCI-H460 tumor-bearing mice. (A and B) Observed (symbol) and predicted (line) profiles of tumor growth by the developed PBPK-PD model in NCI-H460 tumor-bearing mice during multiple intravenous doses of DPT treatment [(A) every 3 days; (B) three times a week]. Symbols represent mean ± S.D. of observations [(A) $n = 6$; (B) $n = 12$ or 6] that came from the present (A) and previous (B) study (Wu et al., 2013). The day of first administration was designated as time zero. (C and D) The relationship between mean observed and predicted tumor volumes at each time point in (A and B) above, respectively. Solid and dashed lines indicate unity and 2-fold errors of prediction, respectively.

could both dynamically reflect the antiproliferation activity and be extended to predict in vivo pharmacodynamics. In vitro NCI-H460 cell proliferation was satisfactorily characterized by the model with stable estimations similar to a previous report (Wu et al., 2013).

Pharmacokinetic characteristics of DPT in NCI-H460 tumor-bearing mice were investigated. The estimated plasma CL values in tumor-bearing mice following two doses were similar (136.68 ml/min per kilogram for 6.25 mg/kg and 138.54 ml/min per kilogram for 25.0 mg/kg), but significantly higher than that in Institute of Cancer Research (ICR) mice (67.73 ml/min per kilogram for 25.0 mg/kg), and were accompanied by a higher distribution volume and a shorter half-life (Chen et al., 2016). It was also found that CL values of DPT in NCI-H460 tumor-bearing mice were larger than hepatic blood flow rate, demonstrating the existence of extrahepatic elimination. However, this phenomenon did not occur in normal mice (Chen et al., 2016). We found that DPT was metabolically stable in both cultured NCI-H460 cells and an homogenate of tumor tissue removed from NCI-H460 tumor-bearing mice, indicating that DPT metabolism did not occur in tumor. It is known that DPT is mainly metabolized by the CYP2C family (Xie et al., 2016), which has an extensive distribution in extrahepatic tissues in mouse (Tsao et al., 2001; Graves et al., 2017). Therefore, the extrahepatic elimination route, which might be urinary excretion or metabolism by an extrahepatic cytochrome P450, needs further investigation. The in vivo pharmacokinetic findings above indicated that the tumor-bearing state might alter characteristics of DPT disposition. Further in vitro studies showed that tumor-bearing mice possess higher intrinsic clearance in hepatic microsomes and lower plasma protein binding compared with normal mice (Chen et al., 2016; Xie et al., 2016). Higher intrinsic clearance in hepatic microsomes, lower plasma protein binding, high distribution in tumor tissue, and existence of extrahepatic elimination might all lead to the higher system clearance and distribution volume of DPT in tumor-bearing mice.

In vivo drug concentration perpetually varies following administration, which is distinguished from the constant level in culture medium. Therefore, a PBPK model established previously (Chen et al., 2016) was introduced to describe the dynamic profiles of DPT in tumor-bearing mice. It was noteworthy that concentration-time profiles in tumor did not synchronize with those in plasma. Although the mechanism leading to the accumulation of DPT in tumor tissue was as yet unknown, the enhanced exposure at the target site undoubtedly facilitated DPT to exert its antitumor efficacy. Since concentration profile in tumor tissue was obviously more meaningful for drug efficacy prediction than that in plasma, a tumor compartment was included in the PBPK model. It was found that pharmacokinetic profiles of DPT in tumor tissues were well characterized by a permeability-limited model rather than perfusion-rate-limited model. It was noticed that mispredictions occurred to some extent in normal tissues, although the predicted exposure ($AUC_{0-120\ minutes}$) in most of the tissues still fell within our 2-fold error criterion. In general, physiologic parameters used in the PBPK model for tumor-bearing mouse were considered similar to those for normal mice (Bradshaw-Pierce et al., 2008; Pawaskar et al., 2013; Zhang et al., 2013). In fact, tumor-bearing state may alter the physiologic parameters and tissue properties, which may become reasons leading to misprediction. However, tumor concentration profiles directly associated with the antitumor effect were better predicted, with most of predicted concentrations falling within 2-fold error, indicating the established PBPK model was still acceptable (Parrott et al., 2005; Guest et al., 2011).

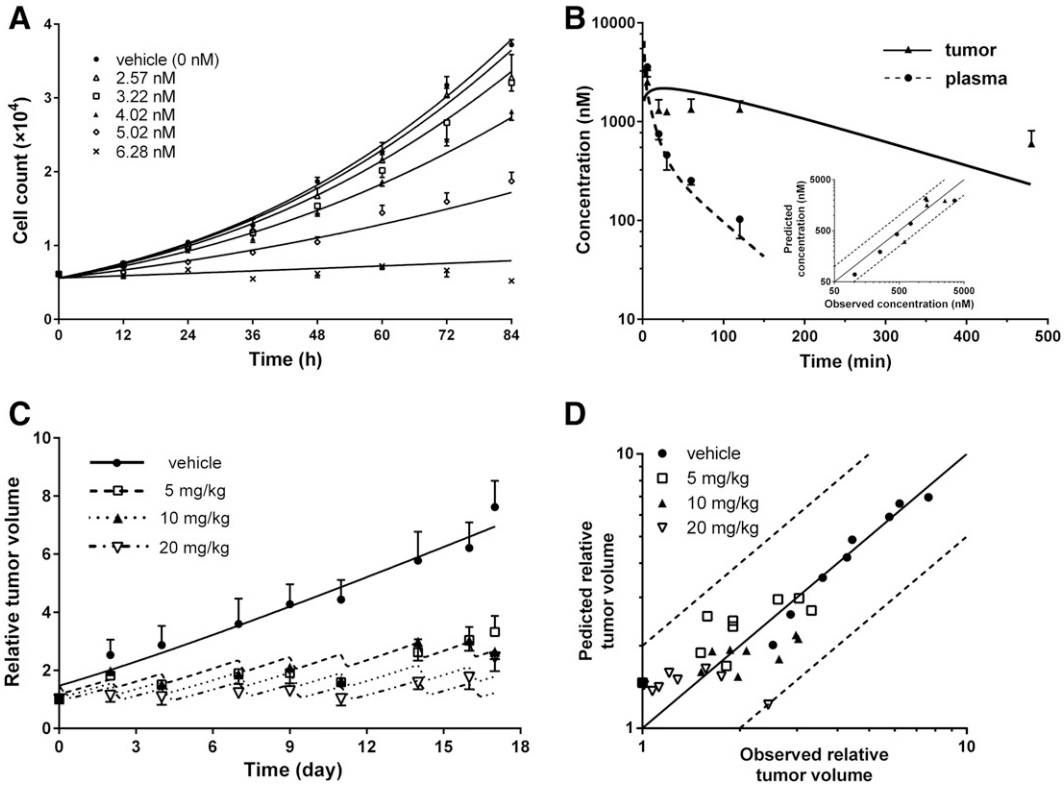

Fig. 7. PBPK-PD model application in SGC-7901 tumor-bearing mice. (A) The observed (symbol) and fitted (line) proliferation profiles of SGC-7901 cells under various concentrations of DPT by the cytotoxicity model extended from two-phase Koch model. Symbols represent mean ± S.D. (n = 5) of cell counts determined by calibration curves. (B) Observed (symbol) and predicted (line) concentration-time profiles of DPT by the developed PBPK model in plasma and tumor of SGC-7901 tumor-bearing mice following a single intravenous dose of 6.25 mg/kg. Symbols represent mean ± S.D. (n = 3) of observations. The inset is the relationship between mean observed and predicted DPT concentrations in plasma and tumor of SGC-7901 tumor-bearing mice at each time point, where solid and dashed lines indicate unity and 2-fold errors of prediction, respectively. (C) Observed (symbol) and predicted (line) profiles of tumor growth by the developed PBPK-PD model in SGC-7901 tumor-bearing mice during multiple intravenous doses of DPT treatment (three times a week). Symbols represent mean ± S.D. (n = 6) of observations that came from the previous study (Wang et al., 2015). The day of first administration was designated as time zero. (D) Relationship between mean observed and predicted relative tumor volumes at each time point in (C). Solid and dashed lines indicate unity and 2-fold errors of prediction, respectively.

Pharmacokinetic profiles of DPT in tumor tissue during multidose DPT treatment were simulated by the developed PBPK model. It is worth mentioning that free drug concentration at the target site may have a closer link to antitumor efficacy than total concentration. Therefore, the unbound concentration profile of DPT in tumor tissue was considered for incorporation into the model and presumed to directly account for the tumor growth inhibition. To predict the pharmacodynamics in tumor-bearing mice on the basis of in vitro assays, the in vivo pharmacodynamic model and parameters were considered the same as the in vitro ones. In fact, we fit the in vivo model (eq. 6) using perturbed tumor growth data of the present study, and the estimated in vivo pharmacodynamic parameters (EC_{50}: 10.8 nM, E_{max}: 0.887 day^{-1}, and γ: 7.00) turned out to be close to in vitro ones (EC_{50}: 8.97 nM, E_{max}: 0.820 day^{-1}, and γ: 7.13), showing consistency between in vitro and in vivo pharmacodynamics. To avoid accidental success, multifaceted in vivo observations were used to validate the efficacy prediction. For the NCI-H460 xenograft model, predicted perturbed-tumor-growth curves were expected to coincide with the observations of both the present study and literature, although dosage regimens and natural growth parameters (λ_0 and λ_1) differed fundamentally between the two datasets, demonstrating the reliable and reasonable prediction of the model approach. What's more, the developed PBPK-PD model was further applied to predict perturbed tumor growth of the SGC-7901 xenograft model from corresponding in vitro evaluations. Consistent with our expectation, a good prediction was obtained, demonstrating the applicability of the proposed model. Pharmacodynamic characteristics and mechanisms of a cytotoxic compound seemed constant between in vitro and in vivo assays of the same cell line, making it possible to predict in vivo antitumor efficacy from in vitro studies, but this remained to be validated with other compounds.

Although many reports demonstrated the application of a PK-PD or PBPK-PD model on antitumor agents, almost all focused on either in vitro or in vivo assays alone (Lobo and Balthasar, 2002; Del Bene et al., 2009; Yuan et al., 2015; Nanavati and Mager, 2017). Those reports developed in vitro or in vivo models separately and seldom related them together, let alone predict in vivo efficacy on the basis of in vitro assays. In our study, we established a novel in vitro pharmacodynamic model that was extendable to prediction of in vivo efficacy, and proposed a PBPK-PD model approach to achieve the prediction, which was subsequently validated by multisourced datasets. To our knowledge, this was the first time a prediction of in vivo antitumor efficacy was obtained for a candidate on the basis of its in vitro evaluation via PBPK-PD model establishment. Natural growth parameters (λ_0 and λ_1) of the targeted tumor were and may still be needed during the prediction with this model, but they could be derived from databases instead. The proposed predictive approach could facilitate dosage regimen design for the in vivo evaluation stage, when in vitro pharmacodynamic data are available. In addition, in the face of quantities of candidates with different antitumor activity levels in the early phase of drug discovery, the present approach may help to predict their in vivo efficacy rapidly

and identify those most promising, as well as the tumor types most sensitive, thus accelerating the discovery process.

In summary, the quantitatively extended preclinical evaluations of DPT deepened our understanding of the links existing between in vitro and in vivo pharmacodynamics. We proposed a predictive PBPK-PD model approach by which antitumor efficacy of DPT in tumor-bearing mice was successfully predicted on the basis of in vitro pharmacodynamics, demonstrating that in vitro cytotoxic assays and quantitative models might play a significant role in forecasting antitumor efficacy in vivo.

Acknowledgments

The authors thank Jiangsu Key Laboratory of Carcinogenesis and Intervention for support with the feeding of and experimentation with tumor-bearing mice.

Authorship Contributions

Participated in research design: Chen, Zhao, L. Liu, X. Liu.

Conducted experiments: Chen, Zhao, F. Liu, Li, Hong.

Contributed new reagents or analytic tools: F. Liu, Li, Hong.

Performed data analysis: Chen, Zhao, Zhong, X. Liu.

Wrote or contributed to the writing of the manuscript: Chen, Zhao, Li, Zhong, L. Liu.

References

Bradshaw-Pierce EL, Steinhauer CA, Raben D, and Gustafson DL (2008) Pharmacokinetic-directed dosing of vandetanib and docetaxel in a mouse model of human squamous cell carcinoma. *Mol Cancer Ther* **7**:3006–3017.

Chen GM, Hu N, Liu L, Xie SS, Wang P, Li J, Xie L, Wang GJ, and Liu XD (2011) Pharmacokinetics of verapamil in diabetic rats induced by combination of high-fat diet and streptozotocin injection. *Xenobiotica* **41**:494–500.

Chen Y, Zhao K, Liu F, Xie Q, Zhong Z, Miao M, Liu X, and Liu L (2016) Prediction of deoxypodophyllotoxin disposition in mouse, rat, monkey, and dog by physiologically based pharmacokinetic model and the extrapolation to human. *Front Pharmacol* **7**:488.

Del Bene F, Germani M, De Nicolao G, Magni P, Re CE, Ballinari D, and Rocchetti M (2009) A model-based approach to the in vitro evaluation of anticancer activity. *Cancer Chemother Pharmacol* **63**:827–836.

Eigenmann MJ, Frances N, Hoffmann G, Lavé T, and Walz AC (2016) Combining nonclinical experiments with translational PKPD modeling to differentiate erlotinib and gefitinib. *Mol Cancer Ther* **15**:3110–3119.

Graves JP, Gruzdev A, Bradbury JA, DeGraff LM, Edin ML, and Zeldin DC (2017) Characterization of the tissue distribution of the mouse*Cyp2c* subfamily by quantitative PCR analysis. *Drug Metab Dispos* **45**:807–816.

Guerram M, Jiang ZZ, Sun L, Zhu X, and Zhang LY (2015) Antineoplastic effects of deoxypodophyllotoxin, a potent cytotoxic agent of plant origin, on glioblastoma U-87 MG and SF126 cells. *Pharmacol Rep* **67**:245–252.

Guest EJ, Aarons L, Houston JB, Rostami-Hodjegan A, and Galetin A (2011) Critique of the two-fold measure of prediction success for ratios: application for the assessment of drug-drug interactions. *Drug Metab Dispos* **39**:170–173.

Hu S, Zhou Q, Wu WR, Duan YX, Gao ZY, Li YW, and Lu Q (2016) Anticancer effect of deoxypodophyllotoxin induces apoptosis of human prostate cancer cells. *Oncol Lett* **12**:2918–2923.

Jiang Z, Wu M, Miao J, Duan H, Zhang S, Chen M, Sun L, Wang Y, Zhang X, Zhu X, et al. (2013) Deoxypodophyllotoxin exerts both anti-angiogenic and vascular disrupting effects. *Int J Biochem Cell Biol* **45**:1710–1719.

Jusko WJ (1971) Pharmacodynamics of chemotherapeutic effects: dose-time-response relationships for phase-nonspecific agents. *J Pharm Sci* **60**:892–895.

Jusko WJ (1973) A pharmacodynamic model for cell-cycle-specific chemotherapeutic agents. *J Pharmacokinet Biopharm* **1**:175–200.

Kelland LR (2004) Of mice and men: values and liabilities of the athymic nude mouse model in anticancer drug development. *Eur J Cancer* **40**:827–836.

Khaled M, Belaaloui G, Jiang ZZ, Zhu X, and Zhang LY (2016) Antitumor effect of Deoxypodophyllotoxin on human breast cancer xenograft transplanted in BALB/c nude mice model. *J Infect Chemother* **22**:692–696.

Khaled M, Jiang ZZ, and Zhang LY (2013) Deoxypodophyllotoxin: a promising therapeutic agent from herbal medicine. *J Ethnopharmacol* **149**:24–34.

Kim Y, Kim SB, You YJ, and Ahn BZ (2002) Deoxypodophyllotoxin; the cytotoxic and anti-angiogenic component from Pulsatilla koreana. *Planta Med* **68**:271–274.

Koch G, Walz A, Lahu G, and Schropp J (2009) Modeling of tumor growth and anticancer effects of combination therapy. *J Pharmacokinet Pharmacodyn* **36**:179–197.

Liu F, Chen Y, Xie QS, Liu L, Xu P, Zhong ZY, and Liu XD (2016) Simultaneous determination of deoxypodophyllotoxin and its major metabolites in rat plasma by a sensitive LC-MS/MS method and its application in a pharmacokinetic study. *Chromatographia* **79**:53–61.

Lobo ED and Balthasar JP (2002) Pharmacodynamic modeling of chemotherapeutic effects: application of a transit compartment model to characterize methotrexate effects in vitro. *AAPS PharmSci* **4**:E42.

Mager DE and Jusko WJ (2001) Pharmacodynamic modeling of time-dependent transduction systems. *Clin Pharmacol Ther* **70**:210–216.

Magni P, Simeoni M, Poggesi I, Rocchetti M, and De Nicolao G (2006) A mathematical model to study the effects of drugs administration on tumor growth dynamics. *Math Biosci* **200**:127–151.

Maurer TS, Debartolo DB, Tess DA, and Scott DO (2005) Relationship between exposure and nonspecific binding of thirty-three central nervous system drugs in mice. *Drug Metab Dispos* **33**:175–181.

Nanavati C and Mager DE (2017) Sequential exposure of bortezomib and vorinostat is synergistic in multiple myeloma cells. *Pharm Res* **34**:668–679.

Parrott N, Paquereau N, Coassolo P, and Lavé T (2005) An evaluation of the utility of physiologically based models of pharmacokinetics in early drug discovery. *J Pharm Sci* **94**:2327–2343.

Pawaskar DK, Straubinger RM, Fetterly GJ, Hylander BH, Repasky EA, Ma WW, and Jusko WJ (2013) Physiologically based pharmacokinetic models for everolimus and sorafenib in mice. *Cancer Chemother Pharmacol* **71**:1219–1229.

Ruggeri BA, Camp F, and Miknyoczki S (2014) Animal models of disease: pre-clinical animal models of cancer and their applications and utility in drug discovery. *Biochem Pharmacol* **87**:150–161.

Salphati L, Wong H, Belvin M, Bradford D, Edgar KA, Prior WW, Sampath D, and Wallin JJ (2010) Pharmacokinetic-pharmacodynamic modeling of tumor growth inhibition and biomarker modulation by the novel phosphatidylinositol 3-kinase inhibitor GDC-0941. *Drug Metab Dispos* **38**:1436–1442.

Shin SY, Yong Y, Kim CG, Lee YH, and Lim Y (2010) Deoxypodophyllotoxin induces G2/M cell cycle arrest and apoptosis in HeLa cells. *Cancer Lett* **287**:231–239.

Sun YN and Jusko WJ (1998) Transit compartments versus gamma distribution function to model signal transduction processes in pharmacodynamics. *J Pharm Sci* **87**:732–737.

Tsao CC, Coulter SJ, Chien A, Luo G, Clayton NP, Maronpot R, Goldstein JA, and Zeldin DC (2001) Identification and localization of five CYP2Cs in murine extrahepatic tissues and their metabolism of arachidonic acid to regio- and stereoselective products. *J Pharmacol Exp Ther* **299**:39–47.

Wang YR, Xu Y, Jiang ZZ, Guerram M, Wang B, Zhu X, and Zhang LY (2015) Deoxypodophyllotoxin induces G2/M cell cycle arrest and apoptosis in SGC-7901 cells and inhibits tumor growth in vivo. *Molecules* **20**:1661–1675.

Wong SK, Tsui SK, Kwan SY, Su XL, and Lin RC (2000) Identification and characterization of Podophyllum emodi by API-LC/MS/MS. *J Mass Spectrom* **35**:1246–1251.

Wu M, Jiang Z, Duan H, Sun L, Zhang S, Chen M, Wang Y, Gao Q, Song Y, Zhu X, et al. (2013) Deoxypodophyllotoxin triggers necroptosis in human non-small cell lung cancer NCI-H460 cells. *Biomed Pharmacother* **67**:701–706.

Xie Q, Chen Y, Liu F, Zhong Z, Zhao K, Ling Z, Wang F, Tang X, Wang Z, Liu L, et al. (2016) Interspecies differences in metabolism of deoxypodophyllotoxin in hepatic microsomes from human, monkey, rat, mouse and dog. *Drug Metab Pharmacokinet* **31**:314–322.

Yong Y, Shin SY, Lee YH, and Lim Y (2009) Antitumor activity of deoxypodophyllotoxin isolated from Anthriscus sylvestris: induction of G2/M cell cycle arrest and caspase-dependent apoptosis. *Bioorg Med Chem Lett* **19**:4367–4371.

Yuan Y, Zhou X, Ren Y, Zhou S, Wang L, Ji S, Hua M, Li L, Lu W, and Zhou T (2015) Semi-mechanism-based pharmacokinetic/pharmacodynamic model for the combination use of dexamethasone and gemcitabine in breast cancer. *J Pharm Sci* **104**:4399–4408.

Zhang T, Li Y, Zou P, Yu JY, McEachern D, Wang S, and Sun D (2013) Physiologically based pharmacokinetic and pharmacodynamic modeling of an antagonist (SM-406/AT-406) of multiple inhibitor of apoptosis proteins (IAPs) in a mouse xenograft model of human breast cancer. *Biopharm Drug Dispos* **34**:348–359.

Address correspondence to: Dr. Li Liu, Center of Drug Metabolism and Pharmacokinetics, School of Pharmacy, China Pharmaceutical University, No.24 Tongjia Lane, Nanjing 210009, China; E-mail: liulee@yeah.net. Or, Dr. Xiaodong Liu, Center of Drug Metabolism and Pharmacokinetics, School of Pharmacy, China Pharmaceutical University, No.24 Tongjia Lane, Nanjing 210009, China; E-mail: xdliu@cpu.edu.cn

Supplemental data

Manuscript title: Predicting anti-tumor effect of deoxypodophyllotoxin in NCI-H460 tumor-bearing mice based on in vitro pharmacodynamics and physiologically based pharmacokinetic-pharmacodynamic model

Authors: Yang Chen, Kaijing Zhao, Fei Liu, Ying Li, Zeyu Zhong, Shijin Hong, Xiaodong Liu and Li Liu

Journal title: Drug Metabolism and Disposition

Supplemental methods

The differential equations in physiologically based pharmacokinetic (PBPK) model of deoxypodophyllotoxin (DPT) in normal tissues of NCI-H460 tumor-bearing mouse

A whole body PBPK model of DPT for tumor-bearing mouse was constructed as the same scheme in the previous report (Chen et al., 2016) except that a tumor compartment was included (Figure 1). It was assumed that DPT was mainly eliminated in liver via transforming to M2 and disposition of DPT in most tissues was illustrated by perfusion-rate limited model. The differential equations in normal tissues were described as follows:

For most of non-elimination tissue compartments (subscript T):

$$V_T \frac{dC_T}{dt} = Q_T \times (C_A - \frac{C_T}{K_{p,T} / R_{bp}}) \tag{1}$$

where C_T (unit: nM), V_T (unit: mL), Q_T (unit: mL/min) and $K_{p,T}$ are the concentration of DPT, the volume, the blood flow rate and tissue-to-plasma concentration ratio of DPT of corresponding tissues, respectively. C_A (unit: nM) means the drug concentration in arterial blood compartment. R_{bp} represents blood-to-plasma concentration ratio, which was assumed to be unity.

For liver compartment (subscript H):

$$\begin{aligned} V_H \frac{dC_H}{dt} = {} & Q_H \times C_A + Q_G \times \frac{C_G}{K_{p,G} / R_{bp}} + Q_S \times \frac{C_S}{K_{p,S} / R_{bp}} \\ & - (Q_H + Q_G + Q_S) \times \frac{C_H}{K_{p,H} / R_{bp}} - PBSF \times \frac{V_{max} \times f_u \times C_H / K_{p,H}}{K_m + f_u \times C_H / K_{p,H}} \end{aligned} \tag{2}$$

where subscripts A, G and S represent arterial blood, gastrointestinal tract and spleen, respectively. Q_H (unit: mL/min) is blood flow rate of hepatic artery. f_u is unbound fraction of DPT in plasma. PBSF (physiological-based scaling factor) is the total hepatic microsomal protein amount of tumor-bearing mouse, which was considered the same as normal mouse (49.28 mg protein/mouse) (Chen et al., 2016). V_{max} (unit: nmol/min/mg protein) and K_m (unit: nM) are the kinetic parameters of M2 formation from DPT in hepatic microsomes of tumor-bearing mice.

For venous blood compartment (subscript V):

$$V_V \frac{dC_V}{dt} = \sum (Q_T \times \frac{C_T}{K_{p,T} / R_{bp}}) - Q_{total} \times C_V \tag{3}$$

For lung compartment (subscript L):

$$V_L \frac{dC_L}{dt} = Q_{total} \times (C_V - \frac{C_L}{K_{p,L} / R_{bp}}) \tag{4}$$

For arterial blood compartment (subscript A):

$$V_A \frac{dC_A}{dt} = Q_{total} \times (\frac{C_L}{K_{p,L} / R_{bp}} - C_A) \tag{5}$$

where Q_{total} (unit: mL/min) is cardiac output.

DPT disposition in brain was illustrated by a permeability-limited model as follows:

$$V_a \frac{dC_a}{dt} = Q_{Br} \times (C_A - C_a) - PS_{Br}(C_a - C_b / K_{p,Br}) \quad (6)$$

and

$$V_b \frac{dC_b}{dt} = PS_{Br} \times (C_a - C_b / K_{p,Br}) \quad (7)$$

where subscript a and b represent vascular and extravascular compartment, which were assumed to account for 3% and 97% of the total brain volume, respectively. C (unit: nM) and V (unit: mL) are DPT concentration and volume of related compartment, respectively. Q_{Br} (unit: mL/min) and $K_{p,Br}$ are blood flow rate of brain and brain-to-plasma concentration ratio of DPT, respectively. PS_{Br} denotes permeability-surface product of brain and was calculated to be 0.0041 mL/min from the value of normal mouse according to the equation: $PS_{Br} = PS_{mouse} \times f_u / f_{u,mouse}$, in which PS_{mouse} and $f_{u,mouse}$ represent the permeability-surface product of normal mouse brain (0.0024 mL/min) and unbound fraction in plasma of normal mouse (2.83%), respectively (Chen et al., 2016). f_u is unbound fraction in plasma of tumor-bearing mouse.

Reference:

Chen Y, Zhao K, Liu F, Xie Q, Zhong Z, Miao M, Liu X, and Liu L (2016) Prediction of Deoxypodophyllotoxin Disposition in Mouse, Rat, Monkey, and Dog by Physiologically Based Pharmacokinetic Model and the Extrapolation to Human. *Front Pharmacol* **7:** 488.

Supplemental figure

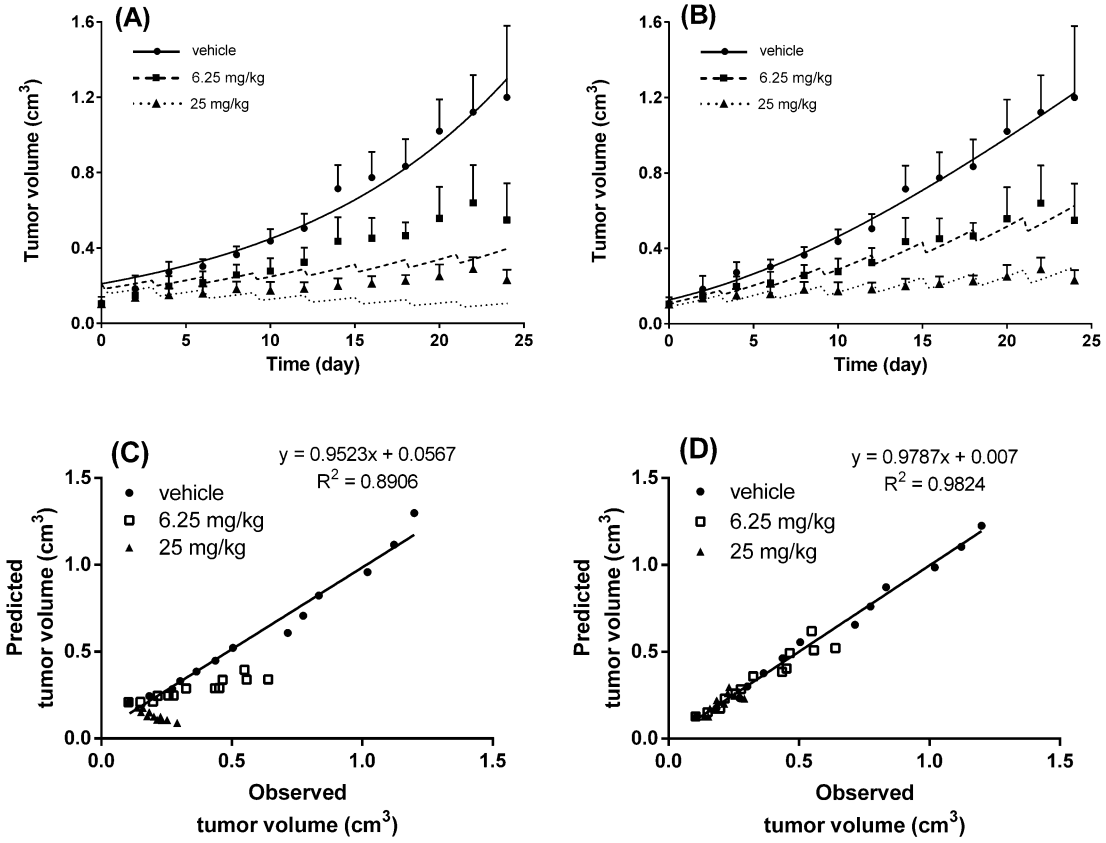

Supplemental Figure. Observed (symbol) and predicted (line) profiles of tumor growth based on exponential model (A) and Koch's two phase model (B) in NCI-H460 tumor-bearing mice during multiple intravenous doses of DPT treatment (every three days) in the present study. Symbols represent mean±SD of observations (n=6). The day of first administration was designated as time zero. (C) and (D) represent the regressions of predicted tumor volumes to mean observed tumor volumes at each time point in (A) and (B), respectively.